Nonlinear electromagnetic response of corrugated metallic gratings

Miriam Gigli,[1,*] Marina Inchaussandague,[1] Claudio Valencia,[2] and Eugenio Méndez[3]

[1]*Grupo de Electromagnetismo Aplicado, Departamento de Física, Facultad de Ciencias Exactas y Naturales, Universidad de Buenos Aires and Instituto de Física de Buenos Aires, Consejo Nacional de Investigaciones Científicas y Te´cnicas Ciudad Universitaria, Pabellón I, C1428EHA Buenos Aires, Argentina*

[2]*Facultad de Ciencias, Universidad Autónoma de Baja California, Km. 105, Carretera Tijuana-Ensenada, Ensenada, B.C. 22860, Mexico*

[3]*División de Física Aplicada, Centro de Investigación Científica y de Educación Superior de Ensenada, Carretera Ensenada-Tijuana No. 3918, Ensenada, B.C. 22860, Mexico*

**Corresponding author: mlg@df.uba.ar*

Received January 4, 2011; revised May 26, 2011; accepted May 26, 2011; posted June 9, 2011 (Doc. ID 140458); published July 18, 2011

We describe a theoretical formalism to study the second-harmonic generation in periodically corrugated surfaces illuminated by a plane wave. The incident wave vector is contained in the plane perpendicular to the grating grooves. Our analysis is based on the most general expression for the nonlinear polarization of a homogeneous and isotropic medium. The diffraction problem is solved using a Rayleigh method, and the numerical technique is illustrated by examples for which the nonlinear susceptibilities are calculated with a free-electron model.

OCIS codes: 190.4350, 240.4350, 050.1950, 240.3695.

1. INTRODUCTION

Surface second-harmonic generation (SHG) has attracted a great deal of attention in recent years and remains the focus of activity of many research groups. The phenomenon provides a powerful spectroscopic tool for the study of the physical and chemical properties of the surfaces of isotropic materials [1–6]. The sensitivity of this nonlinear effect to the state of the surface is due to the fact that, within the dipole approximation, a centrosymmetric material does not produce second-harmonic radiation. At the surface, however, the inversion symmetry is broken, permitting a dipolar contribution to the harmonic field. In addition, SHG microscopy has become an important imaging modality in biomedical optics, because biological tissues such as muscles, tendons, skin dermis, and brain slices are strong generators of second-harmonic signals that can provide valuable information about disease mechanisms [7,8].

The first studies of SHG at interfaces were concerned with the reflection from flat surfaces [9–13]. Later, however, the focus of attention shifted to periodic gratings [14–18] and randomly rough surfaces [19–23]. Among the noteworthy features that have been found are: a strong enhancement of the second-harmonic signal for metallic surfaces in p polarization due to the excitation of surface plasmon polaritons (SPPs) [15–17], and destructive interference effects in the backscattering direction due to multiple scattering [20–23]. More recently, some attention has been given to the problem of SHG by small particles and collections of particles [24–31]. Despite all this work, many aspects of the problem are still not well understood, and the nonlinear interaction of light with rough surfaces and particles remains an active subject of research.

In this paper, we present calculations of the nonlinear electromagnetic response of periodic metallic gratings. For this, we employ the undepleted pump approximation, which allows the decoupling of the Maxwell equations at two frequencies, ω and 2ω. Our formulation is based on the most general expression for the nonlinear polarization of a homogeneous and isotropic medium. In general, the generated second-harmonic field has contributions from the bulk, due to the gradients of the fundamental field in the medium, and the surface, due to the abrupt change in the material properties at the interface. The surface is assumed periodic, and the diffracted linear and nonlinear fields are calculated employing a Rayleigh method [32,33]. To keep the paper to a manageable size, we only present results for the p-polarized second-harmonic intensity obtained when the grating is illuminated by p-polarized light. Usually, this p–p contribution constitutes the most important one.

Numerical techniques based on Green integral theorem [34] have been used to study the nonlinear interaction between electromagnetic waves and randomly rough surfaces [21–23], and would seem suitable for studying periodic surfaces. However, possibly due to truncation effects, the approach encounters difficulties at large angles of incidence and scattering, and when the excitation of SPPs plays a significant role in the interaction [35]. Numerical techniques based on the Rayleigh hypothesis, on the other hand, are simple and efficient, and give reliable results even in cases in which the so-called Rayleigh limit is exceeded [36–39]. They are thus more appropriate for the kind of problems studied here.

It is important to mention that the theoretical formalism presented here is independent of the values or the model employed to determine the nonlinear susceptibilities. This is a significant point because, although there are several theoretical models that provide values for these constants, and there have been experimental attempts to determine them [40],

there is still not sufficient and reliable data in the literature that can be used for calculations with different materials. It is only when we illustrate the results with some examples that we adopt the nonlinear susceptibilities calculated on the basis of a free-electron model [12,41].

The paper is organized as follows: in Section 2 we give details of the formalism used to model SHG for metallic surfaces, Section 3 is devoted to a description of the Rayleigh method employed to calculate the linear and nonlinear fields, in Section 4 we present numerical simulations for silver sinusoidal gratings and analyze the excitation of surface plasmons at the grating interface. Finally, in Section 5 we present our conclusions.

2. THEORY

Let us consider a periodically corrugated boundary between a linear medium (I) and a nonlinear material (II). Both media are isotropic, homogeneous, and nonmagnetic. The permittivity of media I and II are denoted by $\epsilon_{\mathrm{I}}(\omega)$ and $\epsilon_{\mathrm{II}}(\omega)$, respectively. We consider a rectangular coordinate system (x_1, x_2, x_3) in which the grooves of the grating are along the x_2 axis, and the x_3 axis is perpendicular to the mean surface of the grating, pointing toward the linear medium (Fig. 1). The grating is illuminated by a plane wave with harmonic time dependence $\exp(-i\omega t)$.

For the nonlinear medium (II), Maxwell's equations for the fields at 2ω can be written in the form

$$\nabla \times \mathbf{E}(\mathbf{r}|2\omega) = \frac{2i\omega}{c}\mathbf{H}(\mathbf{r}|2\omega), \tag{1a}$$

$$\nabla \times \mathbf{H}(\mathbf{r}|2\omega) = -\frac{2i\omega}{c}\mathbf{D}(\mathbf{r}|2\omega), \tag{1b}$$

$$\nabla \cdot \mathbf{D}(\mathbf{r}|2\omega) = 0, \tag{1c}$$

$$\nabla \cdot \mathbf{H}(\mathbf{r}|2\omega) = 0, \tag{1d}$$

where c is the velocity of light in the vacuum. The constitutive relation for this medium is

$$\mathbf{D}(\mathbf{r}|2\omega) = \epsilon_{\mathrm{II}}(2\omega)\mathbf{E}(\mathbf{r}|2\omega) + 4\pi\mathbf{P}^{\mathrm{NL}}(\mathbf{r}|2\omega), \tag{2}$$

where $\mathbf{P}^{\mathrm{NL}}(\mathbf{r}|2\omega)$ represents the nonlinear polarization.

For isotropic and centrosymmetric media, the first nonzero contribution to the bulk nonlinear polarization is given by the quadrupolar term. The third-order susceptibility tensor has 21 nonzero elements, of which only three are independent. Then, the nonlinear polarization takes the general form [12]

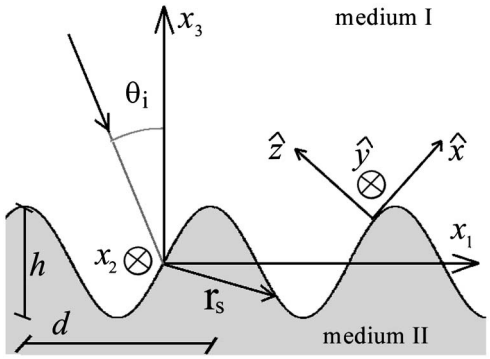

Fig. 1. View of the principal section of the grating.

$$\mathbf{P}^{\mathrm{NL}}(\mathbf{r}|2\omega) = \alpha[\mathbf{E}(\mathbf{r}|\omega)\cdot\nabla]\mathbf{E}(\mathbf{r}|\omega) + \beta\mathbf{E}(\mathbf{r}|\omega)[\nabla\cdot\mathbf{E}(\mathbf{r}|\omega)] + \gamma\nabla[\mathbf{E}(\mathbf{r}|\omega)\cdot\mathbf{E}(\mathbf{r}|\omega)], \tag{3}$$

where $\alpha = \delta - \beta - 2\gamma$, and the constants δ, β, and γ are frequency-dependent parameters characterizing the medium. In a homogeneous medium, the second term on the right hand side of Eq. (3) must always vanish.

Using Maxwell equations and taking into account that the present problem is invariant in the x_2 direction, it is a standard step to demonstrate that all the components of the fields in region I and II can be expressed in terms of the components of the fields along the grooves (E_2 for s polarization and H_2 for p polarization). It has been shown [26] that, if the excitation field is purely s or p polarized, there is no s-polarized second-harmonic radiation. Since we are assuming that the incident field is p polarized, the second-harmonic field will also be p polarized. We shall denote by $\psi_p^{(\mathcal{R})}(\mathbf{r}|\Omega)$, the two component of the magnetic field. Here, $\mathcal{R}$ represents region I or II, and Ω stands for ω or 2ω.

At 2ω, the propagation equation for p polarization in region II is reduced to

$$\left[\nabla_{13}^2 + \left(\frac{2\omega}{c}\right)^2\epsilon_{\mathrm{II}}(2\omega)\right]\psi_p^{(\mathrm{II})}(\mathbf{r}|2\omega) = i4\pi\left(\frac{2\omega}{c}\right)\left(\frac{\partial P_1^{\mathrm{NL}}}{\partial x_3} - \frac{\partial P_3^{\mathrm{NL}}}{\partial x_1}\right), \tag{4}$$

where $\nabla_{13} = \frac{\partial}{\partial x_1}\hat{x}_1 + \frac{\partial}{\partial x_3}\hat{x}_3$ and P_j^{NL} ($j = 1,2,3$) are the rectangular components of the nonlinear polarization vector. From Eq. (3), we find that $\partial P_3^{\mathrm{NL}}/\partial x_1 = \partial P_1^{\mathrm{NL}}/\partial x_3$ and the right hand side of Eq. (4) is zero. This shows that in this case, the bulk contribution to the second-harmonic field vanishes.

To write the boundary conditions that the 2ω fields obey at the interface, it is useful to define a local system of coordinates (x, y, z), as shown in Fig. 1. The boundary conditions can be written as (see [26])

$$\mathbf{E}_t^{(\mathrm{I})}(\mathbf{r}_s|2\omega) - \mathbf{E}_t^{(\mathrm{II})}(\mathbf{r}_s|2\omega) = -4\pi\nabla_t P_z^s(\mathbf{r}_s|2\omega), \tag{5}$$

$$\mathbf{H}_t^{(\mathrm{I})}(\mathbf{r}_s|2\omega) - \mathbf{H}_t^{(\mathrm{II})}(\mathbf{r}_s|2\omega) = 4\pi\left(\frac{2i\omega}{c}\right)\hat{z}\times\mathbf{P}_t^s(\mathbf{r}_s|2\omega), \tag{6}$$

where the subscripts t and z indicate the components that are tangent and normal to the surface, $\mathbf{r}_s$ represents points on the surface, and the superscripts (I) and (II) indicate evaluation from above and below the interface, respectively. In writing Eqs. (5) and (6), we have defined the components of the surface nonlinear polarization as

$$P_z^s(\mathbf{r}_s|2\omega) = \lim_{\tau\to 0}\int_{-\tau}^{\tau}\frac{P_z^{\mathrm{NL}}(\mathbf{r}_s, z|2\omega)}{\epsilon_{\mathrm{II}}(z|2\omega)}\mathrm{d}z, \tag{7}$$

$$\mathbf{P}_t^s(\mathbf{r}_s|2\omega) = \lim_{\tau\to 0}\int_{-\tau}^{\tau}\mathbf{P}_t^{\mathrm{NL}}(\mathbf{r}_s, z|2\omega)\mathrm{d}z. \tag{8}$$

Equations (5) and (6) show that the tangential components of the fields are discontinuous across the interface, in contrast with the more familiar situation found in linear optics. The right hand sides of these equations represent surface sources that can produce radiation at the second-harmonic frequency.

The components of the second-order surface susceptibility tensor χ^{s}_{ijk} relate the amplitudes of the components of the nonlinear surface polarization to the fundamental field amplitudes. For the surface of isotropic material only three distinct components are necessary to characterize the nonlinear response of the system. These are $\chi^{s}_{ttz} = \chi^{s}_{tzt}$, χ^{s}_{ztt}, and χ^{s}_{zzz}. The symmetry properties of the surface enable us to write

$$P^{s}_{z}(\mathbf{r}_s|2\omega) = \chi^{s}_{zzz}[D_z(\mathbf{r}_s|\omega)]^2 + \chi^{s}_{ztt}[\mathbf{E}_t(\mathbf{r}_s|\omega)\cdot\mathbf{E}_t(\mathbf{r}_s|\omega)], \quad (9)$$

$$\mathbf{P}^{s}_{t}(\mathbf{r}_s|2\omega) = \chi^{s}_{ttz}[\mathbf{E}_t(\mathbf{r}_s|\omega)D_z(\mathbf{r}_s|\omega)]. \quad (10)$$

Some simplification occurs for systems that are invariant in one direction (in our case along $x_2 = y$) and are illuminated perpendicular to that direction. In such cases, the problem becomes essentially a scalar one.

To describe the surface profile, we have chosen a parametric representation. The vector valued function $\mathbf{r}_s(t)$ that describes the profile as a function of the parameter t can be written as

$$\mathbf{r}_s(t) = [f(t), g(t)], \quad (11)$$

where the parametric functions $f(t)$ and $g(t)$ are single-valued functions of t. For surfaces that can be represented as single-valued functions of the x_1 coordinate, one can get $f(t) = t = x_1$. In such cases, $g(x_1)$ represents the height of the surface as a function of x_1.

The vectors

$$\mathbf{Z} = [-g'(t), f'(t)], \qquad \mathbf{X} = [f'(t), g'(t)], \quad (12)$$

of magnitude $\phi(t) = \{[f'(t)]^2 + [g'(t)]^2\}^{1/2}$ are normal and tangent to the surface, respectively. The corresponding unit vectors are $\hat{z} = \mathbf{Z}/\phi(t)$ and $\hat{x} = \mathbf{X}/\phi(t)$. Notice that if the parameter t is chosen as the arc length along the curve, $\phi(t) = 1$. Similarly, the operators of unnormalized normal and tangential derivatives are given by

$$\frac{\partial}{\partial \mathbf{Z}} = \left[-g'(t)\frac{\partial}{\partial x_1} + f'(t)\frac{\partial}{\partial x_3}\right], \quad (13a)$$

$$\frac{\partial}{\partial \mathbf{X}} = \left[f'(t)\frac{\partial}{\partial x_1} + g'(t)\frac{\partial}{\partial x_3}\right]. \quad (13b)$$

It should also be mentioned that to evaluate the tangential derivatives on the surface, it is convenient to use the relation

$$\left.\frac{\partial F(\mathbf{r})}{\partial \mathbf{X}}\right|_{\mathbf{r}=\mathbf{r}_s} = \frac{dF(t)}{dt}, \quad (14)$$

which can be obtained by application of the chain rule.

At this stage, it is also convenient to define the values of the field and its normal derivative evaluated on the surface as

$$\psi^{(\mathcal{R})}_{p}(t|\Omega) = \psi^{(\mathcal{R})}_{p}(\mathbf{r}|\Omega)|_{\mathbf{r}=\mathbf{r}_s}, \quad (15a)$$

$$\Upsilon^{(\mathcal{R})}_{p}(t|\Omega) = \left.\frac{\partial \psi^{(\mathcal{R})}_{p}(\mathbf{r}|\Omega)}{\partial \mathbf{Z}}\right|_{\mathbf{r}=\mathbf{r}_s}. \quad (15b)$$

The boundary conditions required to complete the solution for the case of p polarization can be obtained from Eqs. (5) and (6). We find that

$$\frac{1}{\epsilon_{\mathrm{I}}(2\omega)}\Upsilon^{(\mathrm{I})}_{p}(t|2\omega) - \frac{1}{\epsilon_{\mathrm{II}}(2\omega)}\Upsilon^{(\mathrm{II})}_{p}(t|2\omega) = -4\pi\frac{2i\omega}{c}\left[\frac{dP^{s}_{z}(t|2\omega)}{dt} + \frac{\phi(t)P^{\mathrm{NL}}_{x}(t|2\omega)}{\epsilon_{\mathrm{II}}(2\omega)}\right], \quad (16a)$$

$$\psi^{(\mathrm{I})}_{p}(t|2\omega) - \psi^{(\mathrm{II})}_{p}(t|2\omega) = 4\pi\frac{2i\omega}{c}P^{s}_{x}(t|2\omega). \quad (16b)$$

As we have already mentioned, Eq. (4) shows that the bulk contribution to the second-harmonic field vanishes, while Eq. (16) contain nonzero contributions due to the surface. It is worth pointing out, however, that the second term on the right hand side of Eq. (16a) is in fact a mixed term; it has a contribution due to the bulk nonlinear polarization evaluated on the surface.

From Eqs. (3), (9), and (10), the sources of the p-polarized second-harmonic field due to p-polarized excitation can be written as

$$\phi(t)P^{\mathrm{NL}}_{x}(t|2\omega) = -(\alpha/2+\gamma)\frac{c^2}{\omega^2}\left\{\frac{1}{\epsilon^2_{\mathrm{I}}(\omega)}\frac{d}{dt}\left[\frac{\Upsilon^{(\mathrm{I})}_{p}(t|\omega)}{\phi(t)}\right]^2 + \frac{1}{\epsilon^2_{\mathrm{II}}(\omega)}\frac{d}{dt}\left[\frac{1}{\phi(t)}\frac{d\psi^{(\mathrm{I})}_{p}(t|\omega)}{dt}\right]^2\right\} - \frac{\alpha}{2\epsilon_{\mathrm{II}}(\omega)}\frac{d}{dt}[\psi^{(I)}_{p}(t|\omega)]^2, \quad (17a)$$

$$P^{s}_{x}(t|2\omega) = \frac{\chi^{s}_{ttz}}{\epsilon_{\mathrm{I}}(\omega)}\left(\frac{c}{\omega}\right)^2\frac{1}{\phi^2(t)}\Upsilon^{(\mathrm{I})}_{p}(t|\omega)\frac{d\psi^{(\mathrm{I})}_{p}(t|\omega)}{dt}, \quad (17b)$$

$$P^{s}_{z}(t|2\omega) = -\chi^{s}_{zzz}\left(\frac{c}{\omega}\right)^2\left[\frac{1}{\phi(t)}\frac{d\psi^{(\mathrm{I})}_{p}(t|\omega)}{dt}\right]^2 - \chi^{s}_{ztt}\frac{1}{\epsilon^2_{\mathrm{I}}(\omega)}\left(\frac{c}{\omega}\right)^2\left[\frac{\Upsilon^{(\mathrm{I})}_{p}(t|\omega)}{\phi(t)}\right]^2. \quad (17c)$$

3. RAYLEIGH METHOD

We consider that the grating is illuminated from medium I by a p-polarized plane wave of frequency ω propagating along a direction forming an angle θ_i with the x_3 axis (Fig. 1). In what follows, we will assume that medium I is the vacuum. Therefore, the incident magnetic field can be written as

$$\mathbf{H}_i(\mathbf{r}) = \hat{x}_2\psi_0\exp(i\mathbf{k}_i.\mathbf{r}), \quad (18)$$

in which ψ_0 is the amplitude of the incident field and

$$\mathbf{k}_i = \alpha_0\hat{x}_1 - \beta_0\hat{x}_3, \quad (19)$$

where $\alpha_0 = \omega/c\sin\theta_i$ and $\beta_0 = \omega/c\cos\theta_i$.

When the incident wave [Eq. (18)] impinges upon the grating, the reflected field contains the diffracted waves at the fundamental frequency and, under the right conditions, a second-harmonic field is generated by the nonlinearities of the material. We start by writing the x_2 component of the reflected

and transmitted magnetic fields with frequency ω in the regions outside the grooves. It is well known that in these zones, the fields can be represented rigorously by the Rayleigh expansions. Thus, for $x_3 > \max[g(t)]$, we can write

$$\psi_p^{(I)}(\mathbf{r}|\omega) = \sum_{n=-\infty}^{\infty} R_n \exp[i(\alpha_n x_1 + \beta_n x_3)], \tag{20}$$

where

$$\alpha_n = \alpha_0 + \frac{n2\pi}{d}, \tag{21}$$

$$\alpha_n^2 + \beta_n^2 = \epsilon_{\mathrm{I}}(\omega)\left(\frac{\omega}{c}\right)^2. \tag{22}$$

For the region $x_3 < \min[g(t)]$, we have

$$\psi_p^{(\mathrm{II})}(\mathbf{r}|\omega) = \sum_{n=-\infty}^{\infty} T_n \exp[i(\alpha_n x_1 + \gamma_n x_3)], \tag{23}$$

with

$$\alpha_n^2 + \gamma_n^2 = \epsilon_{\mathrm{II}}(\omega)\left(\frac{\omega}{c}\right)^2. \tag{24}$$

The problem of the interaction of light with a diffraction grating between two isotropic, homogeneous, and linear media with permittivities $\epsilon_{\mathrm{I}}(\omega)$ and $\epsilon_{\mathrm{II}}(\omega)$ has been extensively studied using different theoretical methods. In the present paper, the electromagnetic fields of the linear problem are calculated using a standard Rayleigh method [36–39]. Basically, the expansions (Eqs. (20) and (23)) are assumed to be also valid in the region between the grooves (Rayleigh hypothesis). Then, the unknown amplitudes R_n and T_n are found as the numerical solutions of a system of linear equations. Once we have solved the linear problem, Eqs. (20) and (23) are used to calculate the nonlinear sources P_x^{NL}, P_x^s, and P_z^s defined in Eqs. (17a)–(17c), respectively.

We now turn to the electromagnetic fields of frequency 2ω. As the grating surface is periodic with period d, these fields are pseudoperiodic with respect to x_1. Therefore, outside the modulation region, they can also be represented rigorously by the Rayleigh expansions. As we mentioned, for the case we are considering, there is no *s*-polarized second-harmonic radiation. The x_2 component of the magnetic field in the region $x_3 > \max[g(t)]$ can be written as

$$\psi_p^{(\mathrm{I})}(\mathbf{r}|2\omega) = \sum_{n=-\infty}^{\infty} S_n \exp[i(\alpha'_n x_1 + \beta'_n x_3)], \tag{25}$$

where

$$(\alpha'_n)^2 + (\beta'_n)^2 = \epsilon_{\mathrm{I}}(2\omega)\left(\frac{2\omega}{c}\right)^2, \tag{26}$$

$$\alpha'_n = 2\alpha_0 + \frac{n2\pi}{d}. \tag{27}$$

In the region $x_3 < \min[g(t)]$, we obtain a similar expansion

$$\psi_p^{(\mathrm{II})}(\mathbf{r}|2\omega) = \sum_{n=-\infty}^{\infty} W_n \exp[i(\alpha'_n x_1 + \gamma'_n x_3)], \tag{28}$$

with

$$(\alpha'_n)^2 + (\gamma'_n)^2 = \epsilon_{\mathrm{II}}(2\omega)\left(\frac{2\omega}{c}\right)^2. \tag{29}$$

To solve the electromagnetic problem at 2ω, we invoke again the Rayleigh hypothesis. We will assume that Eqs. (25) and (28) are also valid in the region inside the grooves. We then truncate Eqs. (20), (23), (25), and (28) from $-M$ to M and then substitute these equations into the left hand side of the boundary conditions (Eq. (16)), thus obtaining a system of $2(2M+1)$ equations with $2(2M+1)$ unknowns: amplitudes S_n and S_n ($2M+1$ values each of them). Symbolically, these are given by

$$\begin{bmatrix} u_m \\ v_m \end{bmatrix} = \begin{bmatrix} A_{nm} & B_{nm} \\ C_{nm} & D_{nm} \end{bmatrix} \begin{bmatrix} S_n \\ W_n \end{bmatrix}, \tag{30}$$

where

$$A_{mn} = \int_0^1 \exp[i(\alpha'_n - \alpha'_m)f(t)] \exp(i\beta'_n g(t))\mathrm{d}t, \tag{31}$$

$$B_{mn} = -\int_0^1 \exp[i(\alpha'_n - \alpha'_m)f(t)] \exp(i\gamma'_n g(t))\mathrm{d}t, \tag{32}$$

$$C_{mn} = \int_0^1 h_n(t) \exp[i(\alpha'_n - \alpha'_m)f(t)] \exp(i\beta'_n g(t))\mathrm{d}t, \tag{33}$$

$$D_{mn} = -\frac{1}{\epsilon_{\mathrm{II}}(2\omega)}\int_0^1 k_n(t) \exp[i(\alpha'_n - \alpha'_m)f(t)] \exp(i\gamma'_n g(t))\mathrm{d}t, \tag{34}$$

$$h_n(t) = i[-g'(t)\alpha'_n + \beta'_n f'(t)], \qquad k_n(t) = i[-g'(t)\alpha'_n + \gamma'_n f'(t)], \tag{35}$$

$$\begin{aligned} u_m = \frac{8\pi i c \chi^s_{ttz}}{\omega}\Bigg\{ & -\psi_0^2 \int_0^1 \frac{1}{\phi^2}\mathcal{B}\mathcal{C}E_1(m)\mathrm{d}t \\ & + \psi_0 \sum_n R_n \int_0^1 \frac{1}{\phi^2}(\mathcal{E}_n\mathcal{C} - \mathcal{F}_n\mathcal{B})E_2(n,m)\mathrm{d}t \\ & + \sum_{n,l} R_n R_l \int_0^1 \frac{1}{\phi^2}\mathcal{E}_n\mathcal{F}_l E_3(n,m,l)\mathrm{d}t\Bigg\}, \end{aligned} \tag{36}$$

$$v_m = \frac{16\pi i\omega}{c}\left\{\psi_0^2\int_0^1\left[a_1\left(\frac{\phi'}{\phi^3}\mathcal{C}^2-\frac{1}{\phi^2}\mathcal{C}\mathcal{G}\right)+a_2\left(\frac{\phi'}{\phi^3}\mathcal{B}^2-\frac{1}{\phi^2}\mathcal{B}\mathcal{H}\right)+ia_3\mathcal{C}\right]E_1(m)\mathrm{d}t + \psi_0\sum_n R_n\int_0^1\left[a_1\left(\frac{\phi'}{\phi^3}2\mathcal{C}\mathcal{F}_n-\frac{1}{\phi^2}(\mathcal{C}\mathcal{J}_n+\mathcal{G}\mathcal{F}_n)\right)-a_2\left(\frac{\phi'}{\phi^3}2\mathcal{B}\mathcal{E}_n-\frac{1}{\phi^2}(\mathcal{B}\mathcal{I}_n+\mathcal{H}\mathcal{E}_n)\right)+ia_3(\mathcal{F}_n+\mathcal{C})\right]E_2(n,m)\mathrm{d}t + \sum_{n,l}R_nR_l\int_0^1\left[a_1\left(\frac{\phi'}{\phi^3}\mathcal{F}_n\mathcal{F}_l-\frac{1}{\phi^2}\mathcal{F}_n\mathcal{J}_l\right)+a_2\left(\frac{\phi'}{\phi^3}\mathcal{E}_n\mathcal{E}_l-\frac{1}{\phi^2}\mathcal{E}_n\mathcal{I}_l\right)+ia_3\mathcal{F}_l\right]E_3(n,m,l)\mathrm{d}t\right\}, \quad (37)$$

where $\phi=\phi(t)$, $\phi'=d\phi(t)/dt$ and

$$a_1 = -\frac{c^2}{\omega^2}\left[\chi^s_{zzz}+\frac{\alpha/2+\gamma}{\epsilon_{\mathrm{II}}(2\omega)\epsilon^2_{\mathrm{II}}(\omega)}\right], \quad (38)$$

$$a_2 = -\frac{c^2}{\omega^2}\left[\chi^s_{ztt}+\frac{\alpha/2+\gamma}{\epsilon_{\mathrm{II}}(2\omega)}\right], \quad (39)$$

$$a_3 = -\frac{\alpha}{2\epsilon_{\mathrm{II}}(\omega)\epsilon_{\mathrm{II}}(2\omega)}, \quad (40)$$

$$a_4 = \chi^s_{ztt}+\frac{\gamma}{\epsilon_{\mathrm{II}}(2\omega)}, \quad (41)$$

$$E_1(m) = \exp\left[-i\left(\frac{2\pi}{d}mf(t)+2\beta_0 g(t)\right)\right], \quad (42)$$

$$E_2(n,m) = \exp\left[i\left(\frac{2\pi}{d}(n-m)f(t)+(\beta_n-\beta_0)g(t)\right)\right], \quad (43)$$

$$E_3(n,m,l) = \exp\left[i\left(\frac{2\pi}{d}(n+l-m)f(t)+(\beta_n+\beta_l)g(t)\right)\right]. \quad (44)$$

The functions denoted by the caligraphic letters are functions of parameter t and are given by

$$\mathcal{B}=\alpha_0 g'(t)+\beta_0 f'(t), \qquad \mathcal{C}=\alpha_0 f'(t)-\beta_0 g'(t),$$
$$\mathcal{G}=(\mathcal{C})'+i(\mathcal{C})^2, \qquad \mathcal{H}=(\mathcal{B})'+i\mathcal{B}\mathcal{C},$$
$$\mathcal{E}_j=-\alpha_j g'(t)+\beta_j f'(t), \qquad \mathcal{F}_j(t)=\alpha_j f'(t)+\beta_j g'(t),$$
$$\mathcal{I}_j=(\mathcal{E}_j)'+i\mathcal{E}_j\mathcal{F}_j, \qquad \mathcal{J}_j=(\mathcal{F}_j)'+i(\mathcal{F}_j)^2.$$

In the expressions above, the primes denote derivatives with respect to t.

Once the unknown amplitudes S_n and W_n are calculated, the power carried by each one of the diffracted orders can be found.

Let us define $p_n^{2\omega}$, the ratio between the power of the nonlinear reflected nth order and the square of the incident power

$$p_n^{2\omega} = \frac{|\langle\mathcal{P}_n^{2\omega}\rangle|}{|\langle\mathcal{P}_{\mathrm{inc}}\rangle|^2}, \quad (45)$$

where $\langle\mathcal{P}_n^{2\omega}\rangle$ and $\langle\mathcal{P}_{\mathrm{inc}}\rangle$ indicate the mean values of the Poynting vectors associated to the nonlinear reflected nth order and to the incident wave, respectively.

Analogously, we define p_n^{ω} as the ratio between the power of the linear reflected nth order and the incident power

$$p_n^{\omega} = \frac{|\langle\mathcal{P}_n^{\omega}\rangle|}{|\langle\mathcal{P}_{\mathrm{inc}}\rangle|}, \quad (46)$$

where $\langle\mathcal{P}_n^{\omega}\rangle$ indicates the mean value of the Poynting vector associated to the linear reflected nth order.

4. RESULTS AND DISCUSSION

In this section we present some numerical results for sinusoidal silver gratings. For the permittivity as a function of frequency ($\epsilon_{\mathrm{II}}(\omega)$ and $\epsilon_{\mathrm{II}}(2\omega)$), we have used a best fit to experimental data from Johnson and Christy [42].

The nonlinear susceptibilities employed in the numerical simulations are calculated with a free-electron model, which is relatively simple and leads to analytical expressions for the nonlinear susceptibilities. In this model, the nonlinear polarization takes the form given by Eq. (3), with $\alpha=0$, $\beta=e/(8\pi m_0\omega^2)$, and $\gamma=e^3n_B/(8m_0^2\omega^4)$ [41]. Here, e and m_0 are the electron charge and mass, respectively, and n_B is the bulk electron number density.

From Eqs. (7)–(10), we find

$$\chi^{\mathrm{s}}_{zzz} = -\frac{2}{3}\beta\left[\frac{(\epsilon^R_{\mathrm{II}}(\omega)-1)(\epsilon^R_{\mathrm{II}}(\omega)-3)}{2\epsilon^{R2}_{\mathrm{II}}(\omega)}-\frac{2}{3}\ln\left(\frac{\epsilon^R_{\mathrm{II}}(\omega)}{\epsilon^R_{\mathrm{II}}(2\omega)}\right)\right], \quad (47a)$$

$$\chi^{\mathrm{s}}_{ztt} = 0, \quad (47b)$$

$$\chi^{\mathrm{s}}_{ttz} = \beta\left(\frac{\epsilon^R_{\mathrm{II}}(\omega)-1}{\epsilon^R_{\mathrm{II}}(\omega)}\right). \quad (47c)$$

In these expressions, $\epsilon^R_{\mathrm{II}}(\omega)$ is the real part of the permittivity of the metal and is given by $\epsilon^R_{\mathrm{II}}(\omega)=1-\omega_p^2/\omega^2$, where ω_p is the plasma frequency. In the present model, γ can also be expressed as $\gamma=(\beta/4)\left(1-\epsilon^R_{\mathrm{II}}(\omega)\right)$.

In what follows (unless stated otherwise), we use Eqs. (47a)–(47c) for the calculation of the nonlinear parameters.

To perform the numerical simulations, it is necessary to study the convergence of the results. To do so, the number of terms in the series ($N=2M+1$) was varied from $N=11$ to $N=41$; the value of N chosen for our simulations was $N=17$, a value that ensures the convergence of the results of up to four significant digits.

We have also checked that, in the limit of groove to period ratio $h/d\to 0$, the nonlinear specular reflected power tends to the nonlinear reflected power for planar interfaces. In this case, the reflected power has been calculated using the following expression

$$p = \frac{|\langle \mathcal{P}_{\mathrm{ref}} \rangle|}{|\langle \mathcal{P}_{\mathrm{inc}} \rangle|^2} = \frac{8\pi}{c} \frac{|S(2\omega)|^2}{|\psi_0|^4}, \tag{48}$$

where $\langle \mathcal{P}_{\mathrm{ref}} \rangle$ and $\langle \mathcal{P}_{\mathrm{inc}} \rangle$ are the mean values of the reflected and incident Poynting vectors, respectively, ψ_0 is the amplitude of the incident wave, and $S(2\omega)$ is the reflected amplitude of the magnetic field, which has been derived analytically for planar surfaces.

As is well-known, flat metal-dielectric interfaces can support the propagation of SPP waves. The excitation of such waves is accompanied by a significant enhancement of the electromagnetic field on the surface [43], and the electric field components associated with them satisfy the relation $|E_{x3}/E_{x1}| = \sqrt{-\epsilon_{\mathrm{II}}(\Omega)}$; this means that for good conductors $|E_{x3}| \gg |E_{x1}|$ and, therefore, that the electric field associated to the surface plasmon is mainly perpendicular to the surface. Since this is the direction in which the inversion symmetry is broken, surface plasmons are efficient generators of second-harmonic radiation and have played a prominent role in many studies of SHG by corrugated surfaces.

By solving the homogeneous (without sources) electromagnetic problem of a vacuum-metal planar interface [43,44], one can show that surface plasmons satisfy the dispersion relation $\alpha_p(\Omega) = [\epsilon_{\mathrm{II}}(\Omega)/(1+\epsilon_{\mathrm{II}}(\Omega))]^{1/2}\Omega/c$. Surface plasmons can be excited efficiently with periodic gratings when the x_1 component of the wavevector of a diffracted order coincides with their propagation constant. That is, when

$$\alpha_n = \alpha_0 + n\frac{2\pi}{d} \approx \mathrm{Re}(\alpha_p(\omega)), \tag{49}$$

where n is an integer. Similarly, for the second-harmonic field, one has

$$\alpha'_m = 2\alpha_0 + m\frac{2\pi}{d} \approx \mathrm{Re}(\alpha_p(2\omega)), \tag{50}$$

where m is an integer. As we shall see, the fields calculated with the method described here, demonstrate quite clearly the coupling and decoupling of surface plasmons to several diffracted orders for values of θ_i that are near the theoretical values expected on the basis of the above expressions.

Second-harmonic experiments with corrugated surfaces whose profiles and material properties are known are scarce, and it is not easy to make direct comparisons with published data. For the case of periodic gratings, this situation is caused mainly by the experimental problems for controlling the exact shape of the grooves, by the uncertainties in the linear and nonlinear constants that characterize the metal, and by the difficulties associated with the normalization of the data (often, data is presented in arbitrary units). In our attempts to test the theory described here, we present calculations that can be compared with the experimental results reported in [15].

In Fig. 2, we show results for second-harmonic diffraction by sinusoidal silver gratings, calculated with the nominal parameters corresponding to the experimental data presented in Fig. 4 of [15]. That is, we consider gratings with period $0.556\,\mu$m and groove depths $h = 230$ Å, $h = 350$ Å, and $h = 460$ Å (gratings 1, 2, and 3, respectively). In Fig. 2(a), we plot $p_{-1}^{2\omega}$ as a function of the angle of incidence for angles in the region of the excitation of a surface plasmon at the fundamental frequency ($64° < \theta_i < 65.5°$). For the permittivities of silver, we use $\epsilon_{\mathrm{II}}(\omega) = -59.55 + 1.15i$ and $\epsilon_{\mathrm{II}}(2\omega) = -14.14 + 0.14i$, which are the values obtained by Johnson and Christy for a wavelength of $1.064\,\mu$m [42].

The curves have nearly the same shapes as the corresponding experimental ones (Fig. 4 of [15]). Although the results are in qualitative agreement with the experimental ones, there are differences in the angular position of the peaks, as well as in their relative intensities. The peaks in the $p_{-1}^{2\omega}$ theoretical curves appear at $\theta_M \approx 64.85°$, which is consistent with the value of the surface plasmon propagation constant predicted by the flat surface dispersion relation. The experimental peaks, however, appear at a slightly different angle ($\theta_M \approx 64.3°$. This difference is possibly due to the value of the permittivities used in the calculations. To investigate this assumption, we have also performed numerical simulations using the permittivities given by Palik [45]. These results are shown in Fig. 2(b), where we present $p_{-1}^{2\omega}$ for the same gratings studied in the previous figure but with $\epsilon_{\mathrm{II}}(\omega) = -51.99 + 3.38i$ and $\epsilon_{\mathrm{II}}(2\omega) = -10.18 + 0.83i$. We observe that the peaks shift to the left and that the value of θ_M is closer to that obtained in the experimental measurements.

Concerning the relative heights of the curves, we also observe some differences. While in Fig. 2(a), the relation between the height of the peaks for gratings 1 and 2 is approximately 2.3, this value decreases to 1.3 in Fig. 2(b); the analogous value for the experimental data is approximately 2.2.

The results presented in Figs. 2(a) and 2(b) show that the curves are very sensitive to the values of the permittivity used to describe the metal and illustrate some of the difficulties encountered in the comparison with experimental data. So, considering the uncertainties on the optical properties of the metal, the simple model assumed for the nonlinear polarization in our calculations (free-electron model), and the fact that the gratings profiles used in the measurements are not exactly sinusoidal (as mentioned by Coutaz *et al.* [15]), the level of agreement between our calculations and the experimental results was considered satisfactory.

We have carried out calculations with the corrugated gratings with other periods and amplitudes. In all cases, we have used p-polarized illumination with $\lambda = 1.064\,\mu$m. As examples, we consider sinusoidal silver gratings characterized by $d/\lambda = 1$, and several values of the height to period ratio h/d: namely, $h/d = 0.01$, 0.05, 0.075, and 0.1. As before, we consider a free-electron model and the dielectric constants $\epsilon_{\mathrm{II}}(\omega) \approx -59.55 + 1.15i$ and $\epsilon_{\mathrm{II}}(2\omega) = -14.14 + 0.14i$.

Before discussing the details of the calculations, we present some illustrations that can help in the visualization of the results. In Fig. 3, we show the angular trajectories of the diffraction orders as functions of the angle of incidence. Figure 3(a) corresponds to the case of the fundamental field, while Fig. 3(b) corresponds to the second-harmonic field. One can see that some orders are only present within a range of angles of incidence, and that there are more orders at 2ω. The vertical lines of Figs. 3(a) and 3(b), indicate the angles of incidence for which conditions Eq. (49) or (50) are fulfilled; the diffraction orders involved are indicated in each case.

Figure 4(a) shows p_0^{ω}, calculated through Eq. (46) for $n = 0$, as a function of the angle of incidence θ_i. These curves represent the intensity along the curve corresponding to the zero order in Fig. 3(a). The peak near normal incidence is

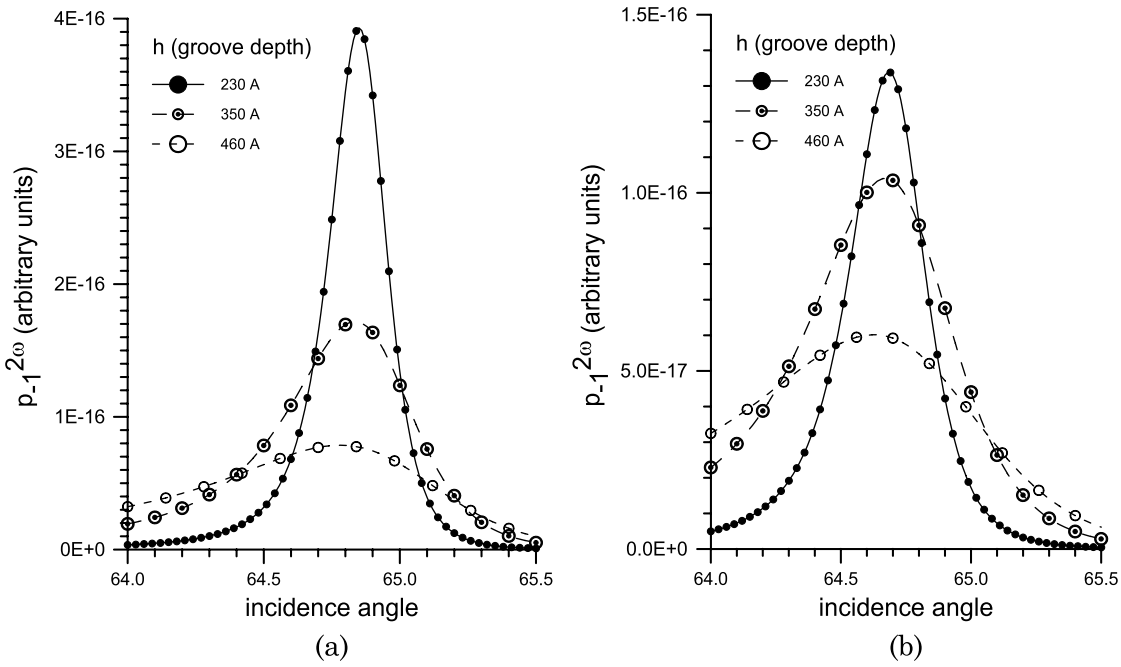

Fig. 2. Computed values of $p_{-1}^{2\omega}$ as a function of the angle of incidence θ_i, for p incidence with $\lambda = 1.064\,\mu$m from the vacuum onto a sinusoidal silver grating with period $d = 0.556\,\mu$m and groove depths $h = 230$ Å, h=350 Å, and $h = 460$ Å (gratings 1, 2, and 3, respectively). These parameters are those used in Fig. 4 of [15]. (a) For the permittivities of silver, we used $\epsilon_{II}(\omega) = -59.55 + 1.15i$ and $\epsilon_{II}(2\omega) = -14.14 + 0.14i$ [42]. (b) For the permittivities of silver, we used $\epsilon_{II}(\omega) = -51.99 + 3.38i$ and $\epsilon_{II}(2\omega) = -10.18 + 0.83i$ [45].

associated to the coupling of a surface plasmon to the (+1) reflected order, and the peak near 82.5° is due to the coupling of a surface plasmon to the (−2) reflected order [see Fig. 3(a)]. As can be observed in the figure, the power diffracted into this order decreases when h/d increases.

The specularly reflected second-harmonic signal $p_0^{2\omega}$, calculated through Eq. (45) for $n = 0$, is plotted in Fig. 4(b) as a function of θ_i. The curves represent the intensities along the curve corresponding to the zero order in Fig. 3(b). Several anomalies are observed in the curve: the peaks at $\theta_i \approx 0.5°$ and at $\theta_i \approx 82.5°$ are related to the already mentioned coupling of the diffracted orders (+1) and (−2) to surface plasmons of frequency ω. In this case, since the excitation of a SPP causes an intensification of the linear fields near the surface, the second-harmonic fields are also enhanced. The same figure shows other anomalies, one near normal incidence ($\theta_i \approx 2°$) and another one at $\theta_i \approx 32.5°$, both corresponding to the coupling of the nonlinear diffracted orders (+2) and (+1), respectively, to SPPs [see Fig. 3(b)]. We observe that the peaks near $\theta_i \approx 82.5°$ become more pronounced when h/d increases. This figure also shows that, for $\theta_i > 48°$, $p_0^{2\omega}$ decreases for greater values of h/d.

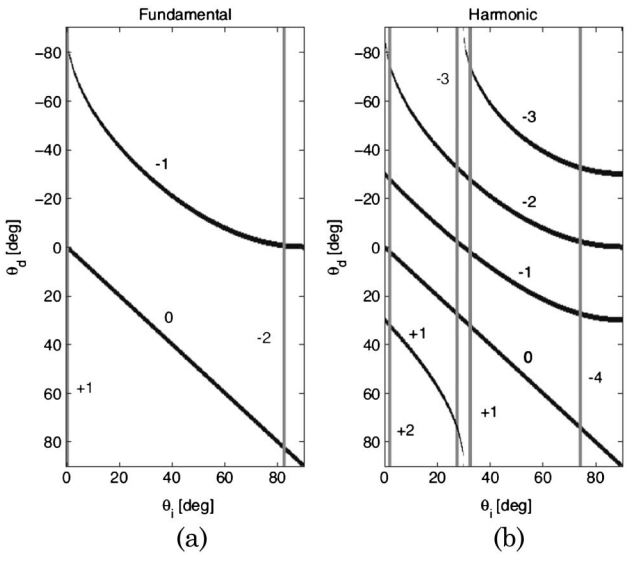

Fig. 3. Angular behavior of the (a) linear and (b) second-harmonic diffraction orders. The curves illustrate the angular position of the various orders as functions of the angle of incidence; the diffraction order is indicated. The vertical lines indicate the angles of incidence for which an order coincides with the surface plasmons propagation constant. The number next to each vertical line indicates the diffraction order involved in the coupling. The wavelength to period ratio is $\lambda/d = 1$, and we have used the dielectric constants $\epsilon_{II}(\omega) \approx -59.55 + 1.15i$ and $\epsilon_{II}(2\omega) \approx -14.14 + 0.14i$.

The fact that the results of Fig. 4(b) indicate that the strongest nonlinear signal occurs for small angles of incidence might seem strange at first sight; this is because the electric field vector of the incident field is nearly parallel to the surface in this case. To understand this result, we first note that the second-harmonic intensity peaks obtained when $\theta_i \approx 0.5°$ coincide with the excitation of a surface plasmon through the (+1) order. This, coupled with the fact that for good conductors $\mathrm{Re}(\alpha_p(2\omega)) \approx 2\mathrm{Re}(\alpha_p(\omega))$, implies that second-harmonic plasmons can be generated efficiently by the nonlinear interaction of plasmons of frequency ω. The interaction of these 2ω plasmons with the grating couples out radiation into the specular direction, as well as in the other diffraction orders. The situation is shown schematically in Fig. 5.

In Fig. 6(a) we plot p_{-1}^{ω} as a function of θ_i. Again, the figure should be interpreted as the intensity along the curve corresponding to the −1 order in Fig. 3(a). This figure shows a strong minimum near normal incidence, associated to the plasmon excited at 0.5°, and another minimum associated

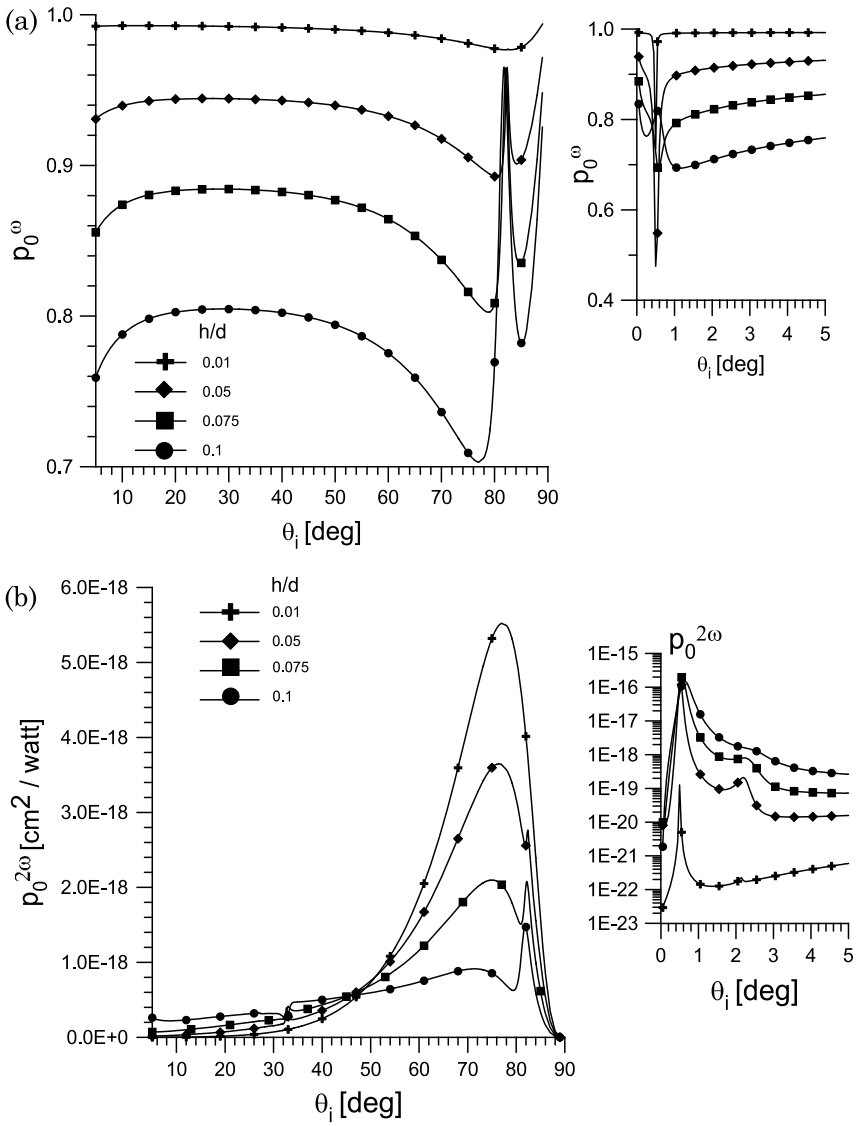

Fig. 4. (a) p_0^{ω} as a function of the angle of incidence θ_i, for p incidence from the vacuum onto a sinusoidal silver grating, $\lambda/d = 1$ and several values of the height to period ratio h/d. On the left, we show p_0^{ω} for $5° < \theta_i < 90°$; on the right, the range $0° < \theta_i < 5°$ is plotted. (b) $p_0^{2\omega}$ as a function of the angle of incidence θ_i. On the left, we show $p_0^{2\omega}$ for $5° < \theta_i < 90°$; on the right, the range $0° < \theta_i < 5°$ is plotted.

to the surface plasmon near 82.5°. It can be appreciated that p_{-1}^{ω} decreases if θ_i increases (except in the region of the two mentioned anomalies), and it increases when h/d increases.

Figure 6(b) shows $p_{-1}^{2\omega}$ as a function of θ_i. This reflected order propagates for all values of $0° < \theta_i < 90°$. As in Fig. 4(b), anomalies corresponding to SPPs at frequencies ω and 2ω are observed. There is also another anomaly, located at $\theta_i \approx 27.5°$, which corresponds to the coupling of a surface plasmon to the (−3)th nonlinear diffracted order. In this figure, and contrary to what is observed in Fig. 4(b) for $p_0^{2\omega}$, for all values of θ_i, $p_{-1}^{2\omega}$ increases if h/d increases.

Figure 7 shows $p_{-2}^{2\omega}$ as a function of θ_i. This reflected order is also propagating for all values of $0° < \theta_i < 90°$. Here we can appreciate the same anomalies observed in Figs. 4(b) and 6(b), corresponding to SPPs at frequency ω. In addition, two minima can be clearly observed at $\theta_i \approx 27.5°$ and $\theta_i \approx 74°$, which correspond to the coupling of a surface plasmon to the (−3)th and (−4)th nonlinear diffracted orders, respectively. These minima are deeper for greater values of h/d.

Figure 8 shows $p_{+1}^{2\omega}$ as a function of θ_i. This reflected order propagates only in the region $0° < \theta_i < 30°$. In this figure, the two surface plasmons near normal incidence can be

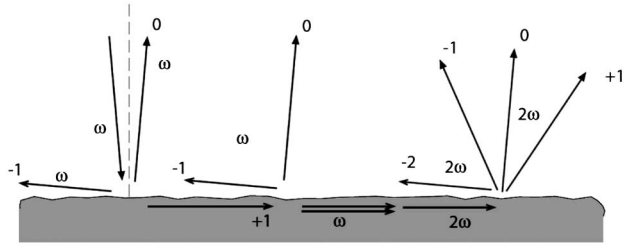

Fig. 5. Schematic diagram of some of the multiple scattering and nonlinear optical processes that can take place in the interaction of the electromagnetic field with the grating. The diagram shows that the specular reflection at the fundamental frequency arises from single and multiple-scattering interactions. Similarly, contributions to the second-harmonic signal can arise from a variety of nonlinear interactions. The figure illustrates the generation of second-harmonic plasmons through the interaction of fundamental plasmons and their subsequent decay into propagating waves.

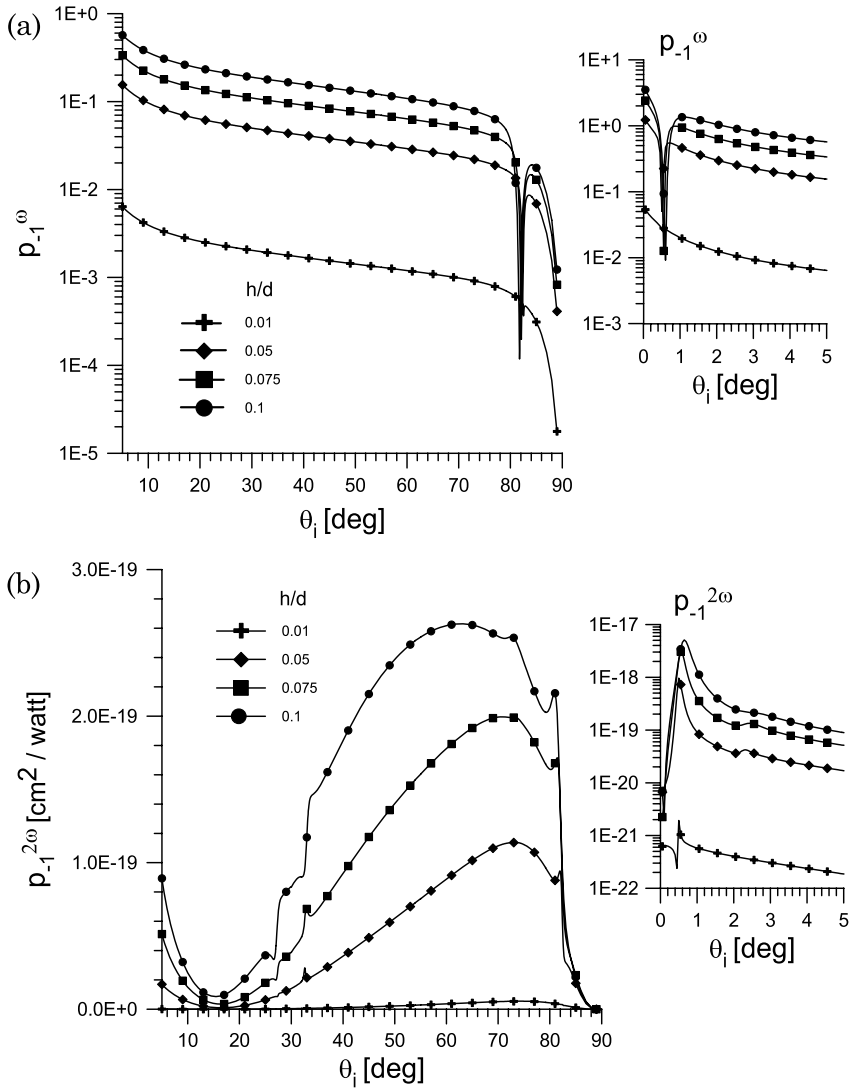

Fig. 6. (a) p^{ω}_{-1} as a function of the angle of incidence θ_i. The parameters are the same as in Fig. 4. On the left, we show p^{ω}_{-1} for $5° < \theta_i < 90°$; on the right, the range $0° < \theta_i < 5°$ is plotted. (b) $p^{2\omega}_{-1}$ as a function of the angle of incidence θ_i. The parameters are the same as in Fig. 4. On the left, we show $p^{2\omega}_{-1}$ for $5° < \theta_i < 90°$; on the right, the range $0° < \theta_i < 5°$ is plotted.

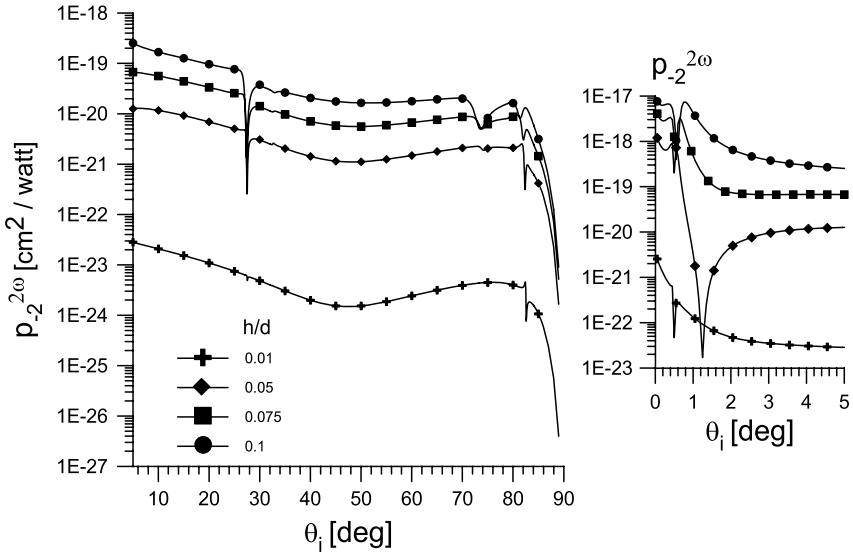

Fig. 7. $p^{2\omega}_{-2}$ as a function of the angle of incidence θ_i. The parameters are the same as in Fig. 4. On the left, we show $p^{2\omega}_{-2}$ for $5° < \theta_i < 90°$; on the right, the range $0° < \theta_i < 5°$ is plotted.

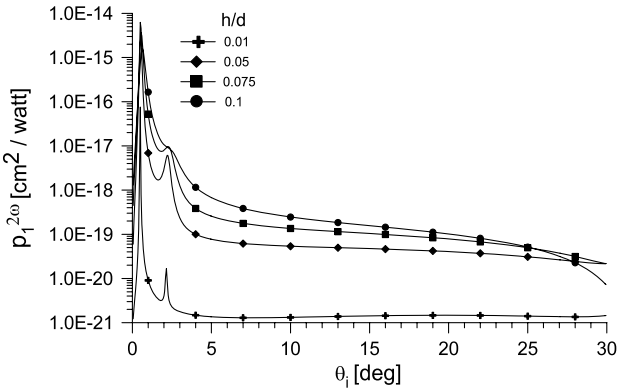

Fig. 8. $p_{+1}^{2\omega}$ as a function of the angle of incidence θ_i. The parameters are the same as in Fig. 4.

appreciated as two sharp maxima. These are the same surface plasmons near normal incidence observed in Figs. 4(b) and 6(b). For $h/d = 0.075$ and $h/d = 0.1$, $p_{+1}^{2\omega}$ decreases if θ_i increases, except in the region near normal incidence. It can also be appreciated that $p_{+1}^{2\omega}$ increases for greater values of h/d.

5. CONCLUSIONS

We have developed a theoretical formalism to study the SHG in periodically corrugated surfaces illuminated by a plane wave, for classical mounting, and based on the most general expression for the nonlinear polarization of an homogeneous and isotropic medium. The diffraction problem was solved using a Rayleigh method, which is efficient and has given reliable results even for grooves with a height to period ratio exceeding the Rayleigh limit for perfect conductors. Our numerical technique was checked for corrugated surfaces, and illustrated by examples for which the nonlinear susceptibilities are calculated with a free-electron model.

ACKNOWLEDGMENTS

Miriam Gigli and Marina Inchaussandague acknowledge financial support from the Universidad de Buenos Aires (grants X848 and X208), Consejo Nacional de Investigaciones Científicas y Técnicas (grant PIP 112-200801-01880), and Agencia Nacional de Promoción Científica y Tecnológica (ANPCyT-BID grant 1728/OC-AR06-01785).

REFERENCES

1. R. M. Corn and D. A. Higgins, "Optical second harmonic generation as a probe of surface chemistry," Chem. Rev. **94**, 107–125 (1994).
2. J. F. McGilp, "Optical characterization of semiconductor surfaces and interfaces," Prog. Surf. Sci. **49**, 1–106 (1995).
3. Y. R. Shen, "Wave mixing spectroscopy for surface studies," Solid State Commun. **102**, 221–229 (1997).
4. G. Lüpke, "Characterization of semiconductor interfaces by second-harmonic generation," Surf. Sci. Rep. **35**, 75–161 (1999).
5. M. C. Downer, B. S. Mendoza, and V. I. Gavrilenko, "Optical second harmonic spectroscopy of semiconductor surfaces: advances in microscopic understanding," Surf. Interface Anal. **31**, 966–986 (2001).
6. Y. Maeda, T. Iwai, Y. Satake, K. Fujii, S. Miyatake, D. Miyazaki, and G. Mizutani, "Optical second-harmonic spectroscopy of Au (887) and Au(443) surfaces," Phys. Rev. B **78**, 075440 (2008).
7. W.-L. Chen, T.-H. Li, P.-J. Su, C.-K. Chou, P. T. Fwu, S.-J. Lin, D. Kim, P. T. C. So, and C.-Y. Dong, "Second harmonic generation χ tensor microscopy for tissue imaging," Appl. Phys. Lett. **94**, 183902 (2009).
8. A. C. Kwan, K. Duff, G. K. Gouras, and W. W. Webb, "Optical visualization of Alzheimer's pathology via multiphoton-excited intrinsic fluorescence and second harmonic generation," Opt. Express **17**, 3679–3689 (2009).
9. F. Brown, R. E. Parks, and A. M. Sleeper, "Nonlinear optical reflection from a metallic boundary," Phys. Rev. Lett. **14**, 1029–1031 (1965).
10. F. Brown and R. E. Parks, "Magnetic-dipole contribution to optical harmonics in silver," Phys. Rev. Lett. **16**, 507–509 (1966).
11. N. Bloembergen, R. K. Chang, and C. H. Lee, "Second harmonic generation of light in reflection from media with inversion symmetry," Phys. Rev. Lett. **16**, 986–989 (1966).
12. N. Bloembergen, R. K. Chang, S. S. Jha, and C. H. Lee, "Optical second-harmonic generation in reflection from media with inversion symmetry," Phys. Rev. B **174**, 813–822 (1968).
13. J. Rudnick and E. A. Stern, "Second harmonic generation from metal surfaces," Phys. Rev. B **4**, 4274–4290 (1971).
14. G. A. Farias and A. A. Maradudin, "Second harmonic generation in reflection from a metallic grating," Phys. Rev. B **30**, 3002–3012 (1984).
15. J. L. Coutaz, M. Nevière, E. Pic, and R. Reinisch, "Experimental study of surface-enhanced second-harmonic generation on silver gratings," Phys. Rev. B **32**, 2227–2232 (1985).
16. E. Popov and M. Nevière, "Surface-enhanced second-harmonic generation in nonlinear corrugated dielectrics: new theoretical approaches," J. Opt. Soc. Am. B **11**, 1555–1564 (1994).
17. A. C. R. Pipino, R. P. Van Duyne, and G. C. Schatz, "Surface-enhanced second-harmonic diffraction: experimental investigation of selective enhancement," Phys. Rev. B **53**, 4162–4169 (1996).
18. D. B. Singh and V. K. Tripathi, "Surface plasmon excitation at second harmonic over a rippled surface," J. Appl. Phys. **102**, 083301 (2007).
19. R. T. Deck and R. K. Grygier, "Surface-plasmon enhanced harmonic generation at a rough metal surface," Appl. Opt. **23**, 3202–3213 (1984).
20. K. A. O'Donnell, R. Torre, and C. S. West, "Observations of backscattering effects in second-harmonic generation from a weakly rough metal surface," Opt. Lett. **21**, 1738–1740 (1996).
21. M. A. Leyva-Lucero, E. R. Méndez, T. A. Leskova, A. A. Maradudin, and J. Q. Lu, "Multiple-scattering effects in the second-harmonic generation of light in reflection from a randomly rough metal surface," Opt. Lett. **21**, 1809–1811 (1996).
22. K. A. O'Donnell and R. Torre, "Second-harmonic generation from a strongly rough metal surface," Opt. Commun. **138**, 341–344 (1997).
23. M. A. Leyva-Lucero, E. R. Méndez, T. A. Leskova, and A. A. Maradudin, "Destructive interference effects in the second harmonic light generated at randomly rough metal surfaces," Opt. Commun. **161**, 79–94 (1999).
24. J. Martorell, R. Vilaseca, and R. Corbalán, "Scattering of second-harmonic light from small spherical particles ordered in a crystalline lattice," Phys. Rev. A **55**, 4520–4525 (1997).
25. N. Yang, W. E. Angerer, and A. G. Yodh, "Angle-resolved second-harmonic light scattering from colloidal particles," Phys. Rev. Lett. **87**, 103902 (2001).
26. C. I. Valencia, E. R. Méndez, and B. S. Mendoza, "Second-harmonic generation in the scattering of light by two-dimensional particles," J. Opt. Soc. Am. B **20**, 2150–2161 (2003).
27. C. I. Valencia, E. R. Méndez, and B. S. Mendoza, "Second-harmonic generation in the scattering of light by an infinite cylinder," J. Opt. Soc. Am. B **21**, 36–44 (2004).
28. Y. Pavlyukh and W. Hübner, "Nonlinear Mie scattering from spherical particles," Phys. Rev. B **70**, 245434 (2004).
29. J. I. Dadap, "Optical second-harmonic scattering from cylindrical particles," Phys. Rev. B **78**, 205322 (2008).
30. A. G. F. de Beer and S. Roke, "Nonlinear Mie theory for second-harmonic and sum-frequency scattering," Phys. Rev. B **79**, 155420 (2009).

31. C. I. Valencia, and E. R. Méndez, "Weak localization effects in the second-harmonic light scattered by random systems of particles," Opt. Commun. **282**, 1706–1709 (2009).
32. L. Rayleigh, "On the dynamical theory of gratings," Proc. R. Soc. A **79**, 399–416 (1907).
33. S. O. Rice, "Reflection of electromagnetic waves from slightly rough surfaces," Commun. Pure Appl. Math. **4**, 351–378 (1951).
34. A. A. Maradudin, T. Michel, A. R. McGurn, and E. R. Méndez, "Enhanced backscattering of light from a random grating," Ann. Phys. **203**, 255–307 (1990).
35. K. A. O'Donnell and E. R. Méndez, "Enhanced specular peaks in diffuse light scattering from weakly rough metal surfaces," J. Opt. Soc. Am. A **20**, 2338–2346 (2003).
36. J. P. Hugonin, R. Petit, and M. Cadilhac, "Plane-wave expansions used to describe the field diffracted by a grating," J. Opt. Soc. Am. **71**, 593–598 (1981).
37. A. Wirgin, "Plane-wave expansions used to describe the field diffracted by a grating: comments," J. Opt. Soc. Am. **72**, 812–813 (1982).
38. R. A. Depine and M. L. Gigli, "Diffraction from corrugated gratings made with uniaxial crystals: Rayleigh methods," J. Mod. Opt. **41**, 695–715 (1994).
39. R. A. Depine and M. L. Gigli, "Conversion between polarization states at the sinusoidal boundary of a uniaxial crystal," Phys. Rev. B **49**, 8437–8445 (1994).
40. K. A. O'Donnell and R. Torre, "Characterization of the second-harmonic response of a silver-air interface," New J. Phys. **7**, 154–164 (2005).
41. J. E. Sipe and G. I. Stegeman, "Nonlinear optical response of metal surfaces," in *Surface Polaritons*, V. M. Agranovich and D. L. Mills, eds. (North-Holland, 1982), pp. 661–701.
42. P. B. Johnson and R. W. Christy, "Optical constants of the noble metals," Phys. Rev. B **6**, 4370–4379 (1972).
43. H. Raether, *Surface Plasmons on Smooth and Rough Surfaces and on Gratings* (Springer, 1988).
44. A. D. Boardman, ed., *Electromagnetic Surface Modes* (Wiley, 1982).
45. E. D. Palik, *Handbook of Optical Constants of Solids* (Academic, 1985).